Comparison of Known PD Signals With the Developed and Commercial HFCT Sensors

S. Birlasekaran, *Senior Member, IEEE*, and Weng Hoe Leong

***Abstract*—Increasing need of cost effective identical sensors for partial discharge (PD) location prompted us to take up this research study. Four high-frequency current transformers (HFCT) were assembled and its performances with a used commercial sensor were compared with the known type of PD signals. In this paper, the responses due to surface, oil corona and air corona are analyzed. PD occurrence in 20 ms period and the shape of single PD with more sampled data points are characterized using seven techniques. The study indicates that HFCT with biflar winding is more sensitive in identifying different types of known PD. The number of turns and gauge of the used wire in HFCT play a role in increasing the sensitivity of PD detection.**

***Index Terms*—Cluster analysis, condition monitoring, HFCT, partial discharge, phase distribution, signal processing, time-frequency transformation, wave shape of single PD, weibull distribution.**

I. Introduction

PARTIAL discharges for condition monitoring of different power apparatus are identified using a variety of sensors like epoxy-mica capacitor, high-frequency current transformer with capacitive (HFVS) or magnetic (HFCT) coupling, Rogowski coil, stator slot coupler, transient earth voltage probe, ultrasonic acoustic sensors and other resonant circuits [1]. The review paper [2] discusses the analysis for PD diagnosis in different industrial equipments. Out of these sensors, HFCT is portable, cost effective and non-intruding type of sensor. Recent work on identifying the location of PD on power network [3] motivated us to take up this work to come up with the simple, identical, and multiple sensors for PD identification and location. Literature [4], [5] reported the comparative performance of different sensors with laboratory controlled conditions. No detailed comparison study is reported with different analysis. The usage of nonconventional air core instrument transformer known as Rogowski coil with shields is recommended to prevent RF interference [6]. The sensitivity of PD detection with these devices is found to be very low especially in apparatus with oil and epoxy insulation. The shields made of copper and aluminum can by pass the external common mode RF interference by capacitive coupling. One needs a proper grounding to achieve this. In the industry, one has to use long coaxial leads for simultaneous measurements which restrict to get common ground. Also, it is found that any metallic interface is found to degrade the high-frequency responses. Our field experience on the calibration of measured PD level using different HFCTs with commercial calibrators suggested that the calibration factors are dependent on the rise time of the used calibration signal. Hence, a simple HFCT with a high permeability core is taken up in this study to understand the role of self and mutual impedances. This paper focuses on the role of winding wound on toroidal ferrite core [7]. The features on the performance of different HFCTs for the same PD with different signal processing techniques are analyzed and the requirement of winding layout and its characteristics for practical PD measurement are identified. It is found that on line PD detection, recognition, discrimination and identifying the location of its occurrence in the electrical equipment connected in power network can be done effectively if one takes into account this HFCT characterization. This principle can be extended to split core current transformer and other purposely designed rectangular core sensors for wider practical use.

Manuscript received May 26, 2006; revised October 26, 2006. Paper no. TPWRD-00285-2006.

S. Birlasekaran is with Queensland University of Technology, Brisbane, Australia-4001 (e-mail: s.birla@qut.edu.au).

W. H. Leong is with the Hoestar Inspection International Pte Ltd., Singapore 347923.

Color versions of one or more of the figures in this paper are available online at http://ieeexplore.ieee.org.

Digital Object Identifier 10.1109/TPWRD.2007.899795

II. HFCT

Four HFCTs (CT1, CT2, CT3, and CT4) on ferrite core [7] were assembled by varying the number of turns, gauze of the wire and winding layout. CT1 to CT3 used one direction winding. CT1 and CT2 had 35 turns with gauze wires 18 and 20, respectively. While CT3 used gauze wire 20 with 40 turns. CT4 used biflar winding with gauze wire 20. 40 turns were laid in one direction of current flow and another 40 turns were laid to have the same current flow in the opposite direction. For comparison study, CT5, commercial HFCT type CAE 140/100 [8] was used as it resulted in good PD prediction in our field investigations with other nonintruding transient earth voltage probe [9] during the last four years. Using an impedance bridge, the impedance characteristic of the wound winding in the form of series inductance (Ls) and series resistance (Rs) was measured and the variation with frequency was plotted in Fig. 1. While Fig. 2 shows the measured transfer impedance characteristics of CT4. It is found to have a bandwidth of more than 100 MHz with two dips. On the average, a transfer function known as figure of merit 11 mV/mA is obtained with CT4. It is found that CT4 with biflar winding offered the minimum self impedance to get the maximum current for magnetic coupling and a wide transfer impedance bandwidth. Using this type of sensor development, the distortion introduced due to sensor and other electronics is reduced and the maximum PD sensitivity is achieved.

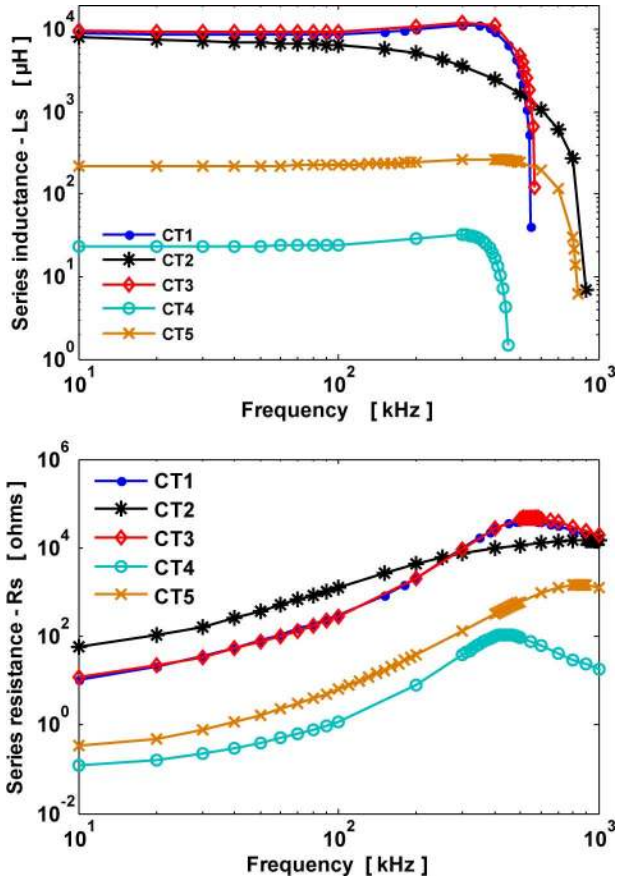

Fig. 1. Variation of Ls and Rs of the windings with frequency.

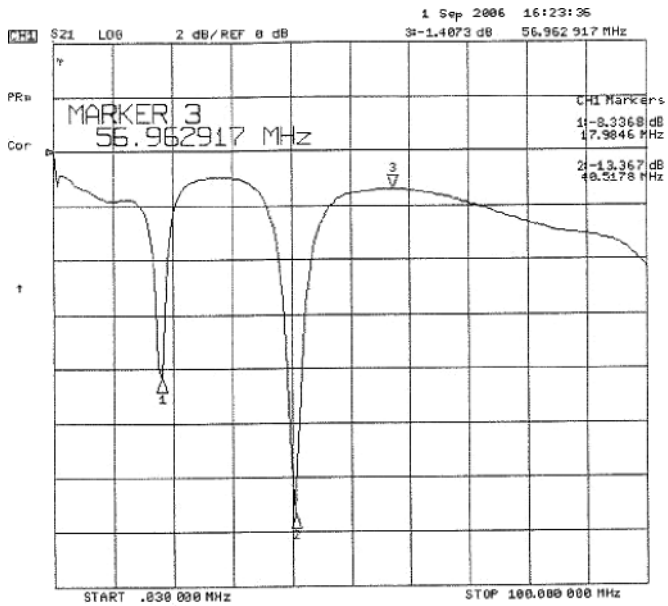

Fig. 2. Measured transfer impedance (S21) characteristic of CT4.

III. Test Arrangement

To evaluate these HFCTs for detecting PD, a variable high voltage (HV) set up shown in Fig. 3 with three test objects was used. Discharges due to surface PD, oil corona and air corona were studied. The HV level can be easily set and the measurements were made at three low-voltage settings of 80, 100, and 120 V. The system was discharge free on HV connections. In this paper, PD readings recorded at 120 V equivalents to HV of 7500 V were analyzed. Fig. 3 shows the test object with a 'VDE' electrode to get uniform field and a point needle electrode with 8 μm tip to generate air corona. The HV insulated current lead (HV2) from the test object was returned through the centre hole of HFCT. The HFCT winding terminals were terminated with 75 Ω and connected to 4-channel high-frequency oscilloscope [10] through a short length of coaxial cable. At each voltage setting, the data were recorded in 20-ms period either with 100 k or 1 M sampled points by interfacing one HFCT sensor at a time. Five sets of data were recorded for statistical analysis. The data on three test objects was analyzed for the group PD occurrence in the 20-ms period, and for the detailed wave shapes of randomly occurring single PD pulses. For denoising, IEC 60270 [11] recommends using wide-band and narrow-band PD instruments using hardware. It restricts the measurement to a maximum bandwidth of 1 MHz. To improve the performance from low frequency to wider bandwidth of greater than 100 MHz, software digital denoising methods are used without loosing any component of the sensed PD signal. This is very compatible with the recommended IEC method and in addition, it is tested with better PD identification results in the industry.

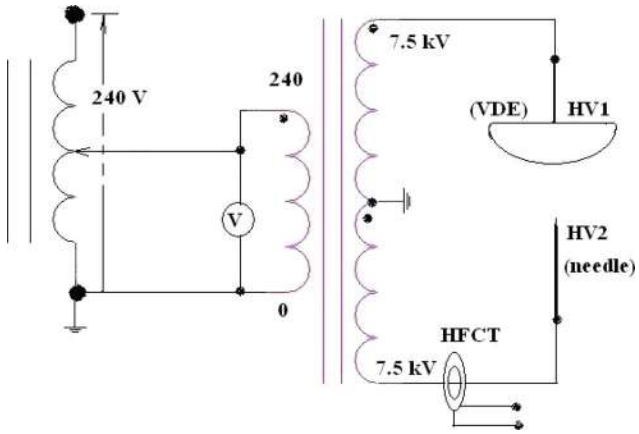

Fig. 3. Layout of HV power supply and electrodes to generate air-corona.

IV. Group PD Occurrence Analysis in 20 ms Period

Random occurring PD pulses in 20-ms period are analyzed traditionally in phase plane [2], [12] for quick interpretation of the type and severity of PD. Reference [2] summarizes the available commercial instrumentation and the results in the form of discharge pulse magnitude (q) and pulse rate (n) analysis, and pulse phase (ϕ) analysis with colorized representation of pulse rate determined with phase windows. Reference [13] reports that the above analysis is depended on the window size used for the determination of n. In this paper, to be compatible with other available tools, the variation of discharge magnitude (q) with phase of occurrence is evaluated. Since pulse rate with q or ϕ will vary with sensor, cumulative number of occurrence is taken for comparative evaluation. In addition, new characterization techniques like the variation of difference between consecutive pulses magnitude (Δq) and time of occurrences (Δt

or delta t) [14], and Weibull distribution of q with cumulative number of occurrence [13], [15] were studied with the PD data collected using sensors.

A. *Signal Processing by* $\mathrm{q}-\phi-\mathrm{n}$ *Analysis*

The sampled responses of 4 sensors at 7.5 kV with 5 cycles of 100 k data in 20 ms (at 5 MS/s) are presented in Fig. 4.

Air Corona (AC): The top four subplots in Fig. 4 show the ac responses taken with one sensor at a time. The response magnitude of the sensor CT1 was found to be minimum and it was similar in response like CT2 with a reduced magnitude. It was found that CT1, CT2, CT3, and CT5 were sensitive to the polarity of current yielding positive pulses in positive half cycle and negative pulses in negative half cycle. CT3 and CT4 had maximum signal magnitudes. CT4 and CT5 were able to pick up the dominant negative corona pulses with high sensitivity [12]. Dominant air corona occurred in limited phase angle interval of 200° to 310°.

Surface PD (S): The middle four subplots in Fig. 4 show the responses due to surface PD. CT4 and CT5 showed the maximum responses and the pulses were distributed in both half cycles. It occurred in two discrete phase ranges. In the positive half cycle, it occurred between 30° to 110°. While in the negative half cycle, it occurred between 210° to 310°. The interval between consecutive pulses was more. The height of the peak pulses varied.

Oil Corona (O): The bottom four subplots in Fig. 4 show the O responses. The discharge magnitudes were almost equal in positive and negative half cycles [12]. Almost equal magnitude pulses occurred in phase angle windows of 30° to 100° and 210° to 280°. It occurred like a burst.

Further presentation concentrated the characteristic features of CT4 and CT5 with a view of industrial application. Then the pulse count was made by picking the peak PD and setting the associated other sampled points of the single pulse to zero. In each sampled 20-ms data, the maximum absolute PD level of q was divided into ten levels. The number of pulses lying in those two consecutive levels was counted and it was plotted with reference to the averaged charge level. About 70 peak pulses above noise level were counted using developed programs for each of five sampled data and they are plotted in Fig. 5. For all the three discharges, CT4 showed a better response with wide PD range as shown by the thin lines. With the logarithmic q plot, CT4 and CT5 had the same rising slope of cumulative number with q but with different origin of q in PD level shown in horizontal axis. The rate of change was more with surface PD and was less for oil-corona. In all the three types of PD, CT4 showed significant response with a wide range of q.

B. *Signal Processing by* $\Delta q-\Delta t$ *Analysis*

References [13], [14] used the distribution of the difference in peak of consecutive PD pulses (Δq as delta q) and the corresponding time interval between those consecutive PD pulses occurrence (Δt as delta time or delta t) for identification of the type of PD in terms of physical ionization processes with increase in applied high voltage. The distribution of these pulses at a voltage was evaluated and the typical response for surface PD is plotted in Fig. 6 for CT4 and CT5. It shows the cluster of plotted points to a period of 0.8 ms. More scatter is seen with

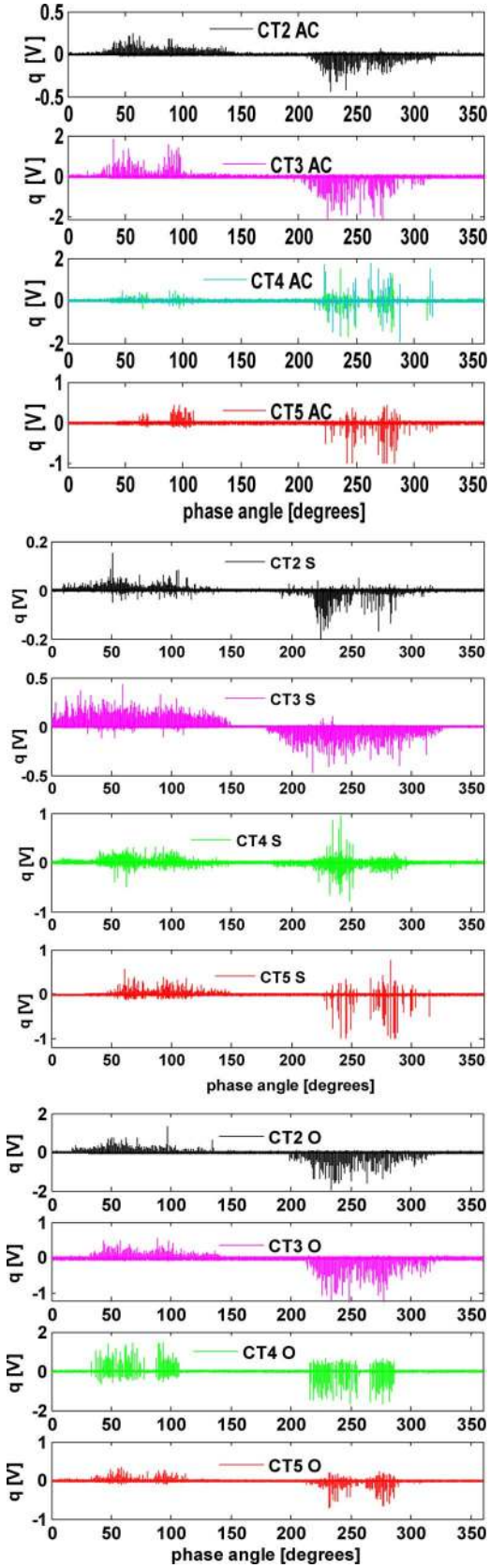

Fig. 4. Response of sensors to air corona, surface, and oil corona at 7.5 kV.

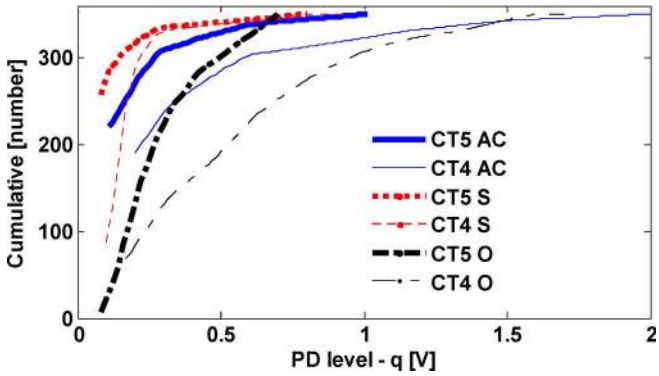

Fig. 5. Variation of cumulative number of occurrence with q for three PDs.

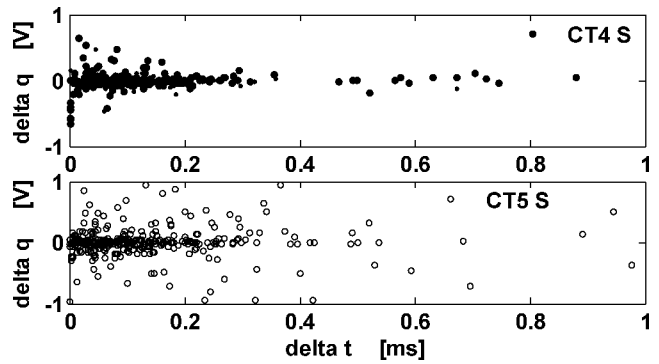

Fig. 6. Variation of Δq with Δt for surface discharge.

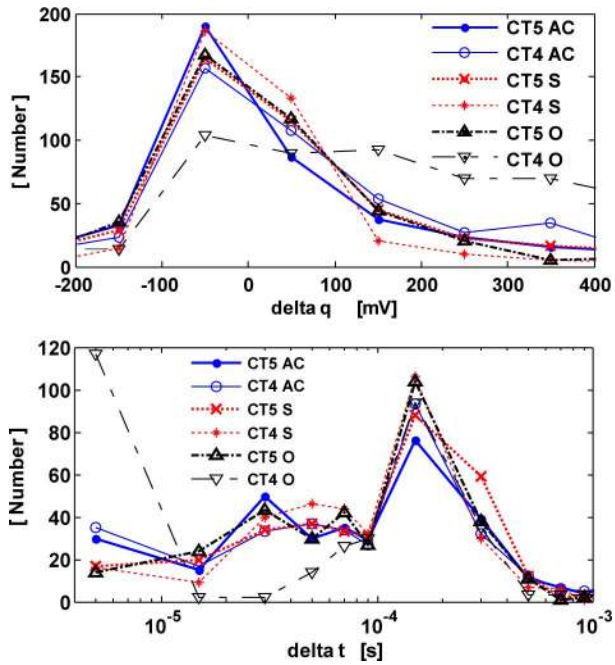

Fig. 7. Number distribution of Δq and Δt dots for various discharges.

CT5. Further quantification was done by counting the number of dots distribution with Δq and Δt, as shown in Fig. 7.

Δq *Distribution:* Nearly 200 of the counted 350 pulses lied around $\Delta q = -50\,\mathrm{mV}$. Other pulses were scattered dominantly in Δq range from -200 mV to $+400$ mV. Air corona at that HV had scatter up to ± 1 V for both CT4 and CT5. Surface PD spread

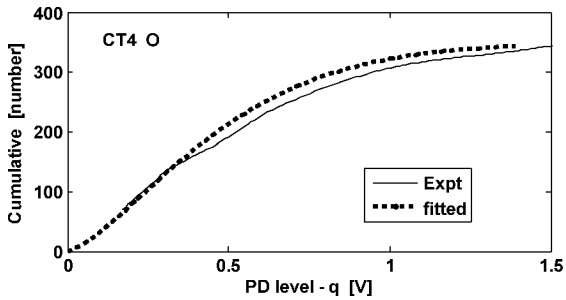

Fig. 8. Fitted Weibull distribution with the measured oil corona using CT4.

TABLE I
VARIATION OF COMPUTED β AND α

Sensor	Type of PD	β	α in volts	Percentage of population
CT5	AC	0.80	0.12	90
CT4	AC	0.87	0.27	80
CT5	O	2.05	0.34	100
CT4	O	1.43	0.52	90
CT5	S	0.67	0.05	90
CT4	S	1.35	0.16	90

up to about $\pm$800 mV. CT5 S had more scatter than CT4 S. Oil corona with CT4 had a wide distribution while CT5 had a range of only $\pm$500 mV. In the analysis, the sampled interval was kept in proportion with number to visualize the distribution clearly.

Δt *Distribution:* Most of the counted 350 pulses had a Δt in the range from 5 μs to 500 μs. Also, it shows there may be two families of pulses. Majority of the pulses lied in duration from 100 to 500 μs. The scatter in Δt was more with air corona using CT5. With oil corona, the scatter in high Δt was minimum. With surface PD, CT4 had less scatter. In conclusion, CT4 was able to provide some clear clusters using Δq and Δt plots with each type of PD.

C. Signal Processing by Weibull Distribution Analysis

Weibull statistical distribution [15] of cumulative number of occurrence (F (q)) with the magnitude of PD (q) was successfully used to identify the type of discharge. The fitted function is given as follows in (1) and (2):

$$F(q_i) = \sum_{i=1}^{\infty} p_i * \left(1 - \exp\left[-\left(\frac{q_i}{\alpha_i}\right)^{\beta_i}\right]\right) \quad (1)$$

$$\sum_{i=1}^{\infty} p_i = 1 \quad (2)$$

where "i" stands for the number of PD types, "q_i" stands for the type of PD magnitude, "β_i" stands for the fitted exponential shape parameter, and "α_i" stands for the fitted scale parameter. Fig. 8 shows the typical fitting made using (1) and (2). Fitted scale and shape parameters for three types of PD using CT4 and CT5 are listed in Table I. The evaluated fitting predicted that there was only one type of dominant PD with the percentage of population lying between 80% to 100%. The scale factor, α indicates that 63% of the cumulative number lies below that value.

It can help us to evaluate the relative sensitiveness of the sensors. It was found that CT4 had higher value for all the discharges in comparison with CT5. While the shape parameter, β helps to identify the type of PD. Air corona had β in the range of 0.8 to 0.87, which was much lower than reported value [15]. CT4 and CT5 had almost identical β values with air corona. Oil corona had high β values in the range of 1.43 and 2.05. For surface PD, the shape factor varied significantly with CT4 and CT5. It suggests that the characterizing shape parameter can vary with the type of sensor.

V. Single PD Wave Shape Analysis

The characteristics of single PD wave shape in time and frequency domains are analysed using signal processing techniques to extract the main features.

A. Time Domain Signal Processing

The PD occurrence in 20 ms is sampled at 50 MS/s in 20 ms so that more number of sampled points can be obtained to study the detailed wave shape of single PD. Using software routines, 70 single pulses with positive and negative peaks were picked for different analysis. Typical observed shapes of the two PD pulses (P1 and P2) are plotted in Fig. 9 for surface, oil corona, and air corona. The peak surface PD magnitude for CT4 varied from 0.15 to 1.05 V in positive and negative peaks. The pulse width varied from 0.1 μs to 5 μs. While for CT5, it varied from 0.05 V to 1 V and the pulse width varied from 0.1 μs to 2 μs. The CT5 oscillation got damped quickly due to high internal resistance.

The peak oil corona magnitude for CT4 varied from 0.2 V to 1.9 V in the positive and negative peaks. The pulsewidth was around 5 μs while for CT5, it varied around 0.175 V and the pulsewidth varied from 0.5 μs to 1 μs. The peak air corona magnitude for CT4 varied from 0.75 V to 2 V in positive and negative peaks. The pulsewidth was around 1 to 4 μs, while for CT5, it varied from 0.2 V to 1 V and the pulsewidth varied from 0.5 μs to 2 μs. In all the three types of PD, CT4 had the high peak magnitude with a sharp rise followed by exponentially decaying oscillatory wave shape in the time domain.

B. Frequency-Domain Signal Processing

The dominant frequency-domain components of single PD responses were extracted and the evaluated power spectral density (PSD) distribution for the corresponding dominant frequency is shown in Fig. 10.

Surface PD: The range of relative PSD distribution was almost same from 0.2 to 30 for both CT4 and CT5 sensors. Cluster in CT4 responses were observed around 400 kHz with positive peaks having more energy. While with CT5, three distributed clusters were observed at 400 kHz, 600 kHz and 20 MHz. Positive peaks had more energy with distribution around 600 kHz.

Oil Corona: The PSD distribution for CT4 was from 1 to 20 while CT5 had a PSD range of 0.01 to 0.7 only. Cluster in CT4 responses was observed at 400 kHz only with two energy levels distribution. With CT5, two clusters were observed at 600 kHz and 20 MHz, respectively.

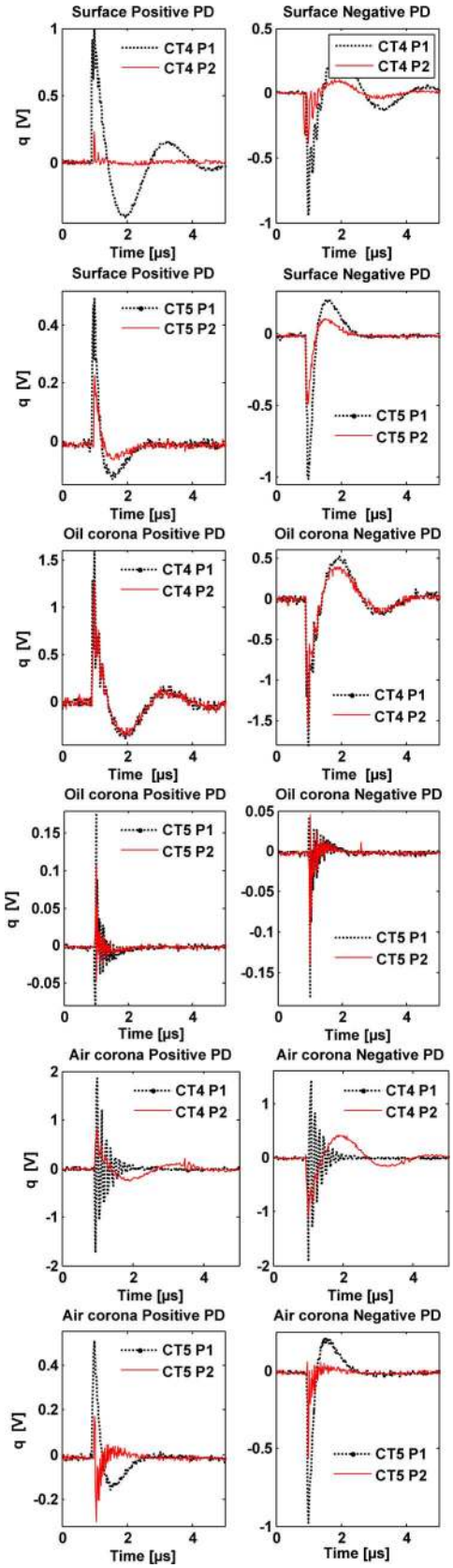

Fig. 9. Typical shapes of two single PD pulses (P1 and P2).

Air Corona: The range of PSD distribution was almost same from 0.03 to 20 for both CT4 and CT5 sensors. Two clusters in

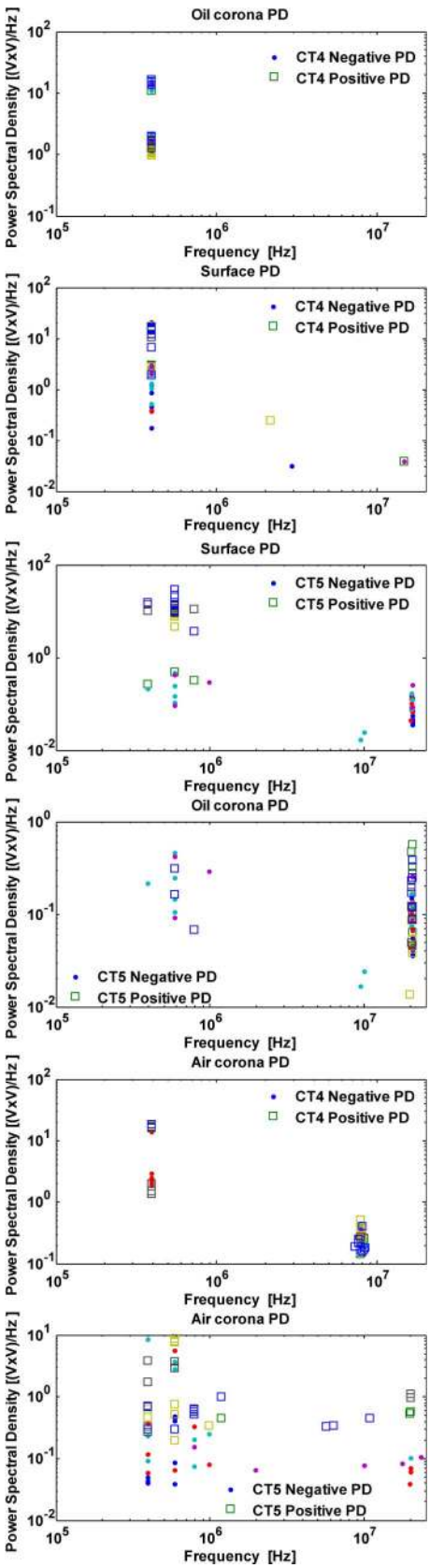

Fig. 10. PSD distribution of 70 single PDs with positive and negative peaks.

CT4 responses were observed around 400 kHz and 8 MHz, respectively. While with CT5, scattered responses were obtained in the frequency range from 400 kHz to 20 MHz.

Using this analysis, it is found that CT4 offered a cluster response with significant PSD values in comparison with CT5 response. In general, positive peaks had higher PSD values in comparison with negative peaks.

C. Time-Frequency Transformation

Cluster in single PD pulses distribution can be characterized by simple time-frequency transformation [16]. This technique is effectively used in identifying noises and other types of PD in different power apparatus [17]. Each single pulse, [y(t)] can be represented by determining its equivalent time length, T, and the equivalent frequency bandwidth, W using (3)–(5)

$$T^2 = \frac{\int_{-\infty}^{\infty} (t - t_0)^2 y^2(t) dt}{\int_{-\infty}^{\infty} y^2(t) dt} \tag{3}$$

$$t_0 = \frac{\int_{-\infty}^{\infty} t.y^2(t).dt}{\int_{-\infty}^{\infty} y^2(t) dt.} \tag{4}$$

In that t_0 represents the averaged value of pulse width. The integrated deviation from that averaged value can be estimated by single T value. Similar logic is applied for frequency domain result. By transforming the time-domain signal to frequency domain, y (f) and frequency content range of the single PD can be determined. Using that, W can be determined using (5)

$$W^2 = \frac{\int_{-\infty}^{\infty} (f)^2 [y(f)]^2 df}{\int_{-\infty}^{\infty} [y(f)]^2 df.} \tag{5}$$

The distribution of the deviated dots for 70 single pulses from the averaged values in the time and frequency ranges is shown in Fig. 11.

Surface PD: The cluster of dots with CT4 response lied in narrow range of T from 0.6 to 0.9 μs with the corresponding W ranging from 1.8 to 5 MHz. It had a wide frequency scatter. While for CT5, T varied widely from 0.35 to 1.5 μs with the corresponding W ranging from 1.8 to 6 MHz.

Oil Corona: Only one crowded cluster is visualized for both CT4 and CT5 sensors. For CT4, T varied between 0.6 to 0.9 μs with the corresponding W ranging from 2.5 to 5 MHz. While CT5 had wide T variation from 0.4 to 1 μs and W variation from 12 to 16 MHz.

Air Corona: More clusters were observed. CT4 had three clusters with first one lying around $T = 0.2$ μs and $W = 8.2$ MHz. The second one lied in T range from 0.7 to 1 μs with W ranging from 2 to 4 MHz. The third cluster was found in T range from 1 to 1.5 μs with W ranging from 10 to 12 MHz.

CT5 had four clusters with the first one lying in T range of 0.35 to 0.5 μs and W range of 2 to 3 MHz. The second, third and fourth clusters were found in T ranges of 0.6 to 1.5 μs, 1.4 to 1.6 μs and 0.7 to 1 μs, respectively. The corresponding W ranges

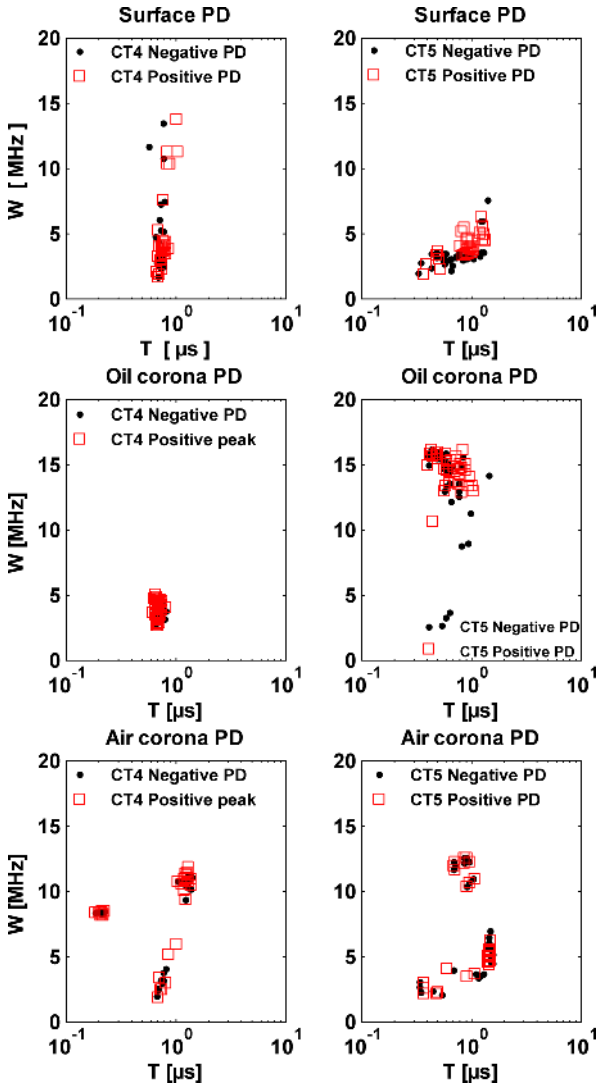

Fig. 11. Distribution of PD clusters in T-W plots.

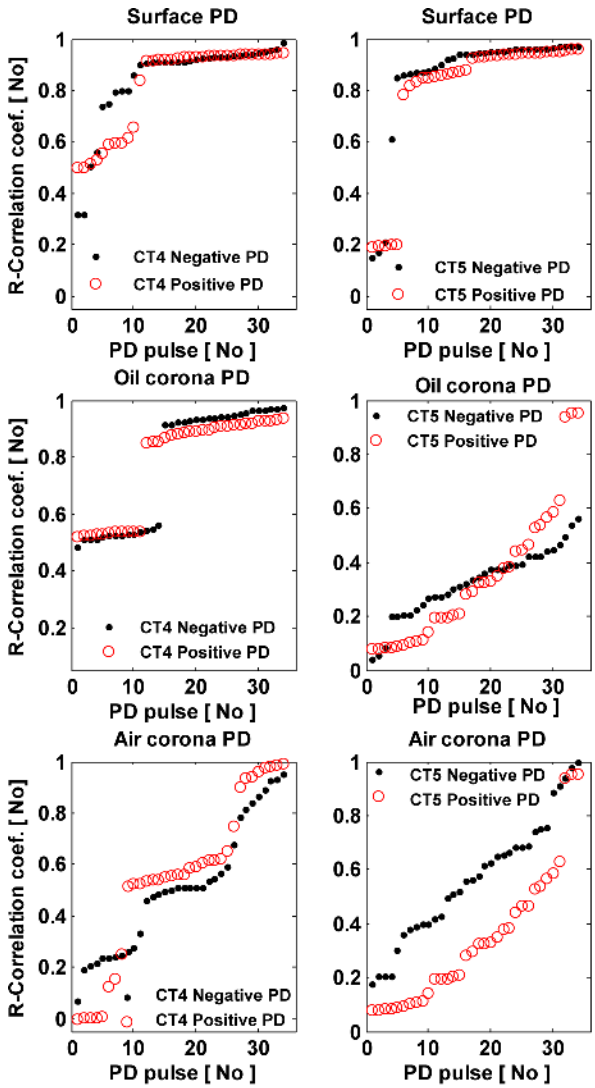

Fig. 12. Correlation factor distribution with respect to one pulse.

were 3–4 MHz, 4.5–7 MHz, and 10–12.5 MHz, respectively. This analysis indicated that CT4 had limited crowded clusters in a definite range to identify the different types of PD.

D. Correlation Factor Between Single Pulses

Correlation factor (R) is another technique used to identify the identical shaped single PD pulses distribution [13]. Extracted 35 single normalized PD pulses in each polarity peak were used. By taking the sampled points of pulse 1 (y1) and one of the remaining 34 pulses (y2), R can be determined by using (6). In that, n represents the number of sampled points. A value of "1" will indicate a positive linear relationship between the two data sets while a value of "0" will indicate no linear relationship between them. A sliding technique is used by appending zeros to get the maximum R for the entire time range

$$\mathrm{R} = \frac{\mathrm{n}\sum(\mathrm{y1})(\mathrm{y2}) - \sum \mathrm{y1} \sum \mathrm{y2}}{\sqrt{\left[\mathrm{n}\sum(\mathrm{y1})^2 - (\sum(\mathrm{y1})^2)\right]\left[\mathrm{n}\sum(\mathrm{y2})^2 - (\sum(\mathrm{y2})^2)\right]}}. \quad (6)$$

A typical distribution of correlation factor by taking the first pulse and the subsequent 34 pulses is shown in Fig. 12. An almost similar distribution is obtained irrespective of the polarity of the peak pulses.

Surface PD: With CT4, 71% of the 34 pulses had R greater than 0.9 in both the polarities with respect to the reference pulse. While, CT5 showed R of greater than 0.8 with 85% of the total pulses. The dominant similar type of single pulses can be separated using this technique.

Oil Corona: CT4 showed a correlation coefficient of greater than 0.85 with 65% of the total pulses, while CT5 had a coefficient greater than 0.9 with 9% of the positive peak pulses.

Air Corona: With CT4, it showed three distinct groups in Fig. 12. 24% of the total pulses had the correlation coefficient greater than 0.8. But CT5 showed that 12% of the total pulses had coefficient greater than 0.9.

This analysis closely compares with the section C results on time-frequency transformation. CT4 is able to separate the similar group in distinct manner as more flat distribution is visualized.

TABLE II
CHARACTERISTIC $q - \Phi - n$ DIFFERENCES IN FIGS. 4 AND 5

Type of PD	CT2	CT3	CT4	CT5
Air corona	q_p - small	q_p - large	q_p - large	q_p - medium
"	sensitive to polarity	sensitive to polarity	insensitive to polarity	sensitive to polarity
"	PD in both half cycles	PD in both half cycles	dominant PD in –ve half cycle	PD in both half cycles
"	less similar q pulses	less similar q pulses	more similar q pulses	less similar q pulses
Surface	q_p - small	q_p - medium	q_p - large	q_p - large
"	wide -Φ occurrence	wide -Φ occurrence	limited -Φ occurrence	limited -Φ occurrence
"	more similar q pulses	more similar q pulses	less similar q pulses	more similar q pulses
Oil corona	q_p - large	q_p - medium	q_p - large	q_p - small
"	-ve half PD dominant	-ve half PD dominant	similar response in both half cycles	similar response in both half cycles
"	wide -Φ occurrence	wide -Φ occurrence	limited -Φ occurrence	limited -Φ occurrence

VI. DISCUSSION

The main objective of this work was to come up with identical sensitive non-intrusive sensors for PD detection and location in any operating HV apparatus. The sensor characterization was done by measuring the impedance characteristics of the sensor up to 100 MHz, as shown in Figs. 1 and 2. The fabricated sensors along with the commercial sensor were tested with the well-known PD sources used in our short courses on PD detection and interpretation.

In our field PD identification approaches, group PD occurrence in a few cycles will be the starting point and the sampling rate was kept as 5 MS/s. Fig. 4 shows the measured PD phase distribution with five cycles of data using three test objects. Table II lists the characteristic features from $q - \Phi - n$ analysis on the four sensors. It should be noted that the PD current signal gets differentiated and will be distorted due to L_s and R_s.

It was found that CT2, CT3, and CT5, with a reduced number of turns, had significant L_s and R_s and the response characteristics varied significantly with each type of discharge. The sensor CT4 with biflar winding and the commercial sensor CT5 presented large PD peak signal responses due to its low self impedance characteristics. For intelligent comparison, the features of the sensed random PD signals on the best performing CT4 and CT5 were analyzed. Fig. 5 showed the trend of the number of pulses with peak-pulse magnitude. CT5 had a sharp change in slope compared to CT4. CT4 had a large peak pulse magnitude range in comparison with CT5.

The distributions of the difference in peak of consecutive PD pulses and the time of occurrence are used to characterize the various discharges in Figs. 6 and 7. Table III compares the responses with CT4 and CT5. CT4 was able to have distribution clusters with less deviation for a type of discharge.

The third technique analyzed the Weibull distribution of the response PD magnitude and the number of PD occurrences. CT4 had high α values in Table I suggesting the existence of maximum sensitivity. It was found that the fitted shape parameter β varied with the sensors and the type of PD. If the apparatus is found to have more number of significant PD activity in a 20-ms period, PD recording is done with high sampling rate in

TABLE III
CHARACTERISTIC $\Delta q - \Delta t$ DIFFERENCES BETWEEN CT4 AND CT5 IN FIGS. 6 AND 7

Type of PD	CT4	CT5
Air corona	$\Delta q > \pm 1$ V	$\Delta q \approx \pm 1$ V
"	90%of Δq points in $\pm$ 0.2 V	90%of Δq points in -0.2 V/0.4 V
"	90%of Δt points in 8 to 400μs	90%of Δt points in 8 to 200μs
"	less Δt scatter beyond 200 μs	more Δt scatter beyond 200 μs
Surface	$\Delta q \approx \pm 0.6$ V	$\Delta q > \pm 0.8$ V
"	90%of Δq points in - 0.2 V/0.28 V	90%of Δq points in ±0.15 V
"	90%of Δt points in 8 to 350μs	90%of Δt points in 8 to 450μs
Oil corona	$\Delta q > \pm 1$ V	$\Delta q \approx \pm 0.6$ V
"	90%of Δq points in - 0.5 V/0.8 V	90%of Δq points in - 0.2 V/0.25 V
"	90%of Δt points in 5 to 400μs	90%of Δt points in 5 to 500μs

TABLE IV
CHARACTERISTIC DIFFERENCES IN PD RESPONSES IN FIG. 9

Type of PD	CT4	CT5
Air corona	Vp≈±0.2 to 2 V	Vp ≈ ± 0.2 to 1 V
"	under-damped oscillation	critically damped oscillation
"	Pulse width ≈ 1 to 2 μs	Pulse width ≈ 0.1 to 0.3 μs
Surface	Vp≈±0.2 to 1 V	Vp≈±0.25 to 1 V
"	under-damped oscillation	critically damped oscillation
"	Pulse width ≈ 0.2 to 1.8 μs	Pulse width ≈ 0.2 μs
Oil corona	Vp≈±1.2 to 1.6 V	Vp≈±0.1 to 0.2 V
"	under-damped oscillation	under-damped oscillation
"	Pulse width ≈ 1.8 μs	Pulse width ≈ 1 μs

TABLE V
CHARACTERISTIC DIFFERENCES IN FIG. 10

Type of PD	CT4	CT5
Air corona	f ≈ 400 kHz & 8 MHz	f ≈ 400 kHz to 25 MHz
"	PSD 400kHz: 1 to 20 8 MHz: 0.1 to 0.6	PSD - .03 to 10 400 kHz to 25 MHz
Surface	f =400 kHz	f ≈ 400 kHz to 20 MHz
"	PSD 400kHz: 0.2 to 15	PSD - .003 to 30 400 kHz to 20 MHz
Oil corona	f ≈ 400 kHz	f ≈ 600 kHz to 20 MHz
"	PSD 400kHz: 1 to 20	PSD - .02 to 0.6 600 kHz to 20 MHz

TABLE VI
CHARACTERISTIC SINGLE PD DIFFERENCES IN FIG. 11

Type of PD	CT4	CT5
Air corona	W ≈ 2 to 4 MHz, 8.5 MHz, 9 to 12 MHz	W ≈ 2 to 7 MHz, 10 to 12 MHz
"	T≈ 0.2 μs; 0.6 to 1.5 μs	T≈ 0.3 to 1.5 μs
Surface	W ≈ 1.5 to 7 MHz, 10.5 to 13.5 MHz	W ≈ 1.5 to 7 MHz,
"	T≈ 0.6 to 1 μs	T≈ 0.35 to 1.5 μs
Oil corona	W ≈ 2 to 5 MHz	W ≈ 3 to 6 MHz, 12 to 16 MHz
"	T≈ 0.6 to 0.8 μs	T≈ 0.4 to 1.2 μs

TABLE VII
CHARACTERISTIC SINGLE PD CORRELATION COEFFICIENT DISTRIBUTION IN FIG. 12

Type of PD	CT4	CT5
Air corona	R > 0.8 . 24% R > 0.5 . 62% trend same in + and - peaks	R > 0.8 . 15% R > 0.5 . 62% -ve peak high R relative to +ve
Surface	R > 0.8 . 82% R > 0.5 . 94% trend same in + and - peaks	R > 0.8 . 88% R > 0.5 . 91% trend same in + and - peaks
Oil corona	R > 0.8 . 65% R > 0.5 . 99% trend same in + and - peaks	R > 0.8 . 9% R > 0.5 . 24% trend same in + and - peaks

the range of 50 MS/s. Using such data, the detailed shape of single PD can be analyzed with more number of sampled points. About 35 pulses with positive peak and another 35 pulses with negative peak were extracted using software. The main features on single PD wave shape recorded using CT4 and CT5 are compared by another four techniques.

Fig. 9 showed the typical time domain shapes of two PD pulses, P1 and P2. Table IV lists the characteristic differences in single PD time-domain responses. The initial rising or falling edge of PD was sharp followed by decaying oscillatory waveform. The oscillation was damped in CT5 in short duration and it is likely due to the high resistance of the winding. CT4 had a good coupling, resulting in maximum peak magnitude with fast peak response in the range of 100 ns.

Fig. 10 displayed the dominant frequency-domain components. Table V lists the characteristic differences. Responses up to 20 MHz were obtained. CT4 presented better frequency cluster response with high PSD values. Fig. 11 used the time-frequency transformation technique in terms of equivalent time (T) and frequency (W) lengths and its respective deviations of single PD pulses. Table VI compares the responses. CT4 results had limited crowded clusters for each type of known PD. The scattered noise signals beyond the identified PD cluster can be easily removed for denoising.

Correlation factor of each single PD wave shape to others can be used to identify the different similar group of pulses [13]. Table VII compares the percentage variation of the number of pulses with the correlation coefficient. The typical analysis in Fig. 12 revealed CT4 had flat responses to identify the groups of similar PD and noises.

VII. CONCLUSION

Asset management with reliable condition indicators becomes an essential decision process in the present competitive energy market around the world. Smart decision-making sensors are the needed interfacing devices for condition monitoring of HV operating apparatus. The described signal-processing techniques extract the condition indicating features and can locate the developing localized fault by using multi-sensors. With that point of view, this study is taken up.

The study indicated that HFCT with low internal impedance will result in better wide band frequency response. Low resistance can be achieved using thick gauge wires and low inductance can be achieved by biflar winding layout with magnetic core of high permeability. The developed HFCT model CT4 performed well in comparison with the commercial CT5 and other fabricated sensors in detecting the random occurring PD. The seven analyzing methods suggest that denoising and extraction of significant characterizing features for PD type identification can be effectively done using CT4. For identical multisensor development, the characteristics shown in Figs. 1 and 2 can be used to minimize the distortion introduced by the various HFCT sensors.

REFERENCES

[1] T. E. Goodeve, G. C. Stone, and L. Macomber, "Experience with compact epoxy-mica capacitors for rotating machine partial discharge detection," in *Proc. Electrical and Electronics Insulation Conf.*, 1995, pp. 685–689.

[2] G. C. Stone, "Partial discharge diagnostics and electrical equipment insulation condition assessment," *IEEE Trans. Dielectr. Electr. Insul.*, vol. 12, pp. 891–902, Oct. 2005.

[3] Q. Shaozhen and S. Birlasekaran, "The study of PD propagation phenomenon in power network," *IEEE Trans. Power Del.*, vol. 21, no. 3, pp. 1083–1091, Jul. 2006.

[4] Y. Tian, P. L. Lewin, A. E. Davies, S. G. Swingler, S. J. Sutton, and G. M. Hathaway, "Comparison of on-line partial discharge detection methods for HV cable joints," *IEEE Trans. Dielectr. Electr. Insul.*, vol. 9, pp. 604–615, Aug. 2002.

[5] N. H. Ahmed and N. N. Srinivas, "On-line partial discharge detection in cables," *IEEE Trans. Dielectr. Electr. Insul.*, vol. 5, pp. 181–188, Apr. 1998.

[6] M. Muhr, T. Strehl, E. Gulski, K. Feser, E. Gockenbach, W. Hauschild, and E. Lemke, "Sensors and sensing used for non-conventional PD detection," presented at the CIGRE Conf., Paris, France, 2006, Paper No. D1-102, unpublished.

[7] Ferrite core with the RS stock no: 232-9808 and part no. 28-780C36, Catalogue on RS products, Singapore, p. 889, Apr. 2005 to Mar. 2006.

[8] High frequency current transformer type HFCT CAE 140/100, IPEC Engineering, Manchester, U.K.

[9] Transient Earth Voltage Probe, EA Technology Ltd. Chester, U.K.

[10] Tektronix Manual No: 071-0700-01 on TDS 7104 digital phosphor, 4 channel, 1 GHz bandwidth with 10 GS/s oscilloscope.

[11] *Partial Discharge Measurements*, IEC Std. 60270, Int. Electrotech. Comm. (IEC), 2000, Geneva.

[12] *IEEE Guide for Partial Discharge Measurement in Liquid-Filled Power Transformers and Shunt Reactors*, IEEE Std. C57.113-1991, 1992, p. 12.

[13] Y. Ming, "Characterization of Partial Discharge Pulses of Power Generator," Ph.D. thesis, Nanyang Technological Univ., Singapore, 2004.

[14] R. Patsch and D. Benzerouk, "Characterization of partial discharge processes—What parameters work best?," in *Proc. Int. Conf. Solid Dielectrics*, Toulouse, France, Jul. 2004.

[15] A. Contin, G. C. Montanari, and C. Ferraro, "PD source recognition by Weibull processing of pulse height distributions," *IEEE Trans. Dielectr. Electr. Insul.*, vol. 7, pp. 48–58, Feb. 2000.

[16] L. Franks, *Signal Theory*. Englewood Cliffs, NJ: Prentice-Hall, 1969, p. 136.

[17] G. C. Montanari and A. Cavallini, "A new approach to partial discharge testing of HV cable systems," *IEEE Elect. Insul. Mag.*, vol. 22, pp. 14–23, Jan./Feb. 2006.

S. Birlasekaran (M'70–SM'97) was born in Madras, India. He received the Master's degree (with distinction) in high voltage engineering from the Indian Institute of Science, Bangalore, and the Ph.D. degree in transformer insulation from the University of Queensland, Queensland, Australia.

He has about 25 years of work experience in high-voltage engineering. In academics, he has worked at VJTI, India, the University of Queensland and University of New Castle in Australia, and Nanyang Technological University, Singapore. Currently, he is a Principal Research Fellow in the area of asset management of transformers with Queensland University of Technology. He conducted research at CSIRO, Lindfield, Australia. He was a R&D Senior Engineer at Electrodata, Sydney, Australia, and at SEAQ, Northgate, Brisbane, Australia. He has authored about 20 IEEE publications in the area of condition monitoring. He is a professional engineer and consultant.

Dr. Birlasekaran is a member of the ICPADM 2006 committee and a member of the CIGRE panel from Australia. He received the special IEEE High Interest Paper Award from 2004 Surge protection Committee, IEEE (USA).

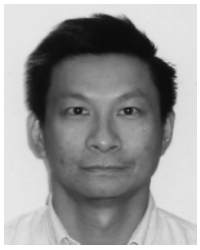

Weng Hoe Leong was born in Singapore and holds an advance diploma in manufacturing. In addition, he has high-level professional certification to do infrared thermography, vibration, and partial discharge analysis and power quality industrial measurements.

He is the Managing Director of Hoestar Inspection International Pte Ltd., Singapore, and Hoestar Reliability Instruments Sdn Bhd. Since 1992, Hoestar has provided the equipment condition inspection services in Singapore, Malaysia, and the region. He is a Representative for Inframetric Inc. USA in this region and is actively involved with research and development work on PD monitoring with Nanyang Technological University, Singapore. Hoestar manufactures PD instruments, conducts a number of short industrial courses, and publishes technical leaflets related to condition monitoring. He also has about ten years of work experience in the Singapore Navy and the Naval Technical Training School.